Research Square

Preprints are preliminary reports that have not undergone peer review.
They should not be considered conclusive, used to inform clinical practice,
or referenced by the media as validated information.

Post-treatment, treatment-pathway-associated remodeling of the gastric microbiome after chemoradiotherapy-immunotherapy and chemoimmunotherapy: predicted functional axes, external host context, and in silico drug prioritization

Jiayang Gong
Nanjing Medical University
Zhe Wang
Nanjing Medical University
Yun Shi
Nanjing Medical University
Minlan Ren
Second Affiliated Hospital of Nanjing Medical University
Tingting Li
Second Affiliated Hospital of Nanjing Medical University
Lingli Huang
Jiangsu Cancer Hospital
Gang Li
Nanjing Medical University
Rui Peng
pengrui@njmu.edu.cn
Nanjing Medical University

Research Article

Keywords: gastric cancer, 16S rRNA, treatment pathway-related microbiome remodeling, chemoradiotherapy combined with immunotherapy, chemotherapy immunotherapy, pathological complete response, PICRUSt2, pharmacogenomics

Posted Date: November 13th, 2026

DOI: https://doi.org/10.21203/rs.3.rs-11431220/v1

License: This work is licensed under a Creative Commons Attribution 4.0 International License.
Read Full License

Additional Declarations: No competing interests reported.

Post-treatment, treatment-pathway-associated remodeling of the gastric microbiome after chemoradiotherapy-immunotherapy and chemoimmunotherapy: predicted functional axes, external host context, and in silico drug prioritization

Jiayang Gong[1],Zhe Wang[1],Yun Shi[1],Minlan Ren[2],Tingting Li[2], Lingli Huang[1]***, Gang Li[1]**,Rui Peng[1]*

1.Department of General Surgery, The Affiliated Cancer Hospital of Nanjing Medical University & Jiangsu Cancer Hospital & Jiangsu Institute of Cancer Research, Nanjing, Jiangsu 210009, China.
2.Medical Center for Digestive Diseases, The Second Affiliated Hospital of Nanjing Medical University, Nanjing, China.

*Correspondence: Department of General Surgery, The Affiliated Cancer Hospital of Nanjing Medical University & Jiangsu Cancer Hospital & Jiangsu Institute of Cancer Research, Nanjing, Jiangsu 210009, China. E-mail address: pengrui@njmu.edu.cn (R. Peng)

**Correspondence: Department of General Surgery, The Affiliated Cancer Hospital of Nanjing Medical University & Jiangsu Cancer Hospital & Jiangsu Institute of Cancer Research, Nanjing, Jiangsu 210009, China. E-mail address: ligang@njmu.edu.cn (G. Li)

***Correspondence: Department of Pharmacy, Jiangsu Cancer Hospital, Jiangsu Institute of Cancer Research, The Affiliated Cancer Hospital of Nanjing Medical University, Nanjing, China. E-mail address: lingli_huang@njmu.edu.cn (L. Huang)

Abstract

Background

Radiotherapy may induce a unique "therapeutic-conditioned" gastric cancer microbiome.We compared two treatment options: chemoradiotherapy combined with immunotherapy (RCI): PGTVp: 30 Gy/12F, PGTVn: 30 Gy/12F + tislelizumab 200 mg + XELOX (oxaliplatin 200 mg, 1 day; capecitabine 1.5 g, once in the morning and evening, for 1–14 days) + PD-1 inhibitor.The control was a chemotherapy immunotherapy (CI) regimen: tislelizumab 200 mg + XELOX (oxaliplatin 200 mg, 1 day; capecitabine 1.5 g, once in the morning and evening, for 1–14 days) + PD-1 inhibitor.We compared microbiome status after RCI and CI, and compared efficacy responses within each treatment pathway.

Method

A total of 91 post-treatment samples were included (CI, n=61; RCI, n=30), stratified by CI-pCR, CI-NR, RCI-pCR, and RCI-NR.We integrated OTU-level Bray-Curtis analysis, CLR-limma classification model, PICRUSt2 prediction, external paired gastric mucosal tissue control set, TCGA-STAD bulk transcriptome, GSE167297 single-cell quality control and annotation, epithelial pseudo-chronology, and GDSC2-targeting compound prioritization.

Result

We found that there are differences between RCI and CI in Shannon index, Simpson index and community structure.The difference is mainly reflected in the fact that bacterial groups such as Exiguobacterium are higher in RCI (q=3.42e-02).We found that the four sets of global tests of CI-pCR, CI-NR, RCI-pCR and RCI-NR supported the difference between Shannon (q=2.43e-02) and Simpson (q=4.31e-02).We find that the difference in global inspection support is mainly driven by RCI-NR.For the RCI-pCR group, the results showed that the

Shannon index was higher (q=4.56e-02).For the CI group, Lactococcus was related to NR (q=2.39e-02).Public data show that tumor tissues have higher species richness and diversity, and Exiguobacterium and others overlap in the screened bacterial groups.External single-cell analysis identified marker-inferred immune and stromal cell populations via QC in 23,310/30,365 cells.Pseudochronological analysis provides exploratory epithelial state continuity.Exiguobacterium is a leading candidate strain in the RCI-pCR direction and can be mapped to the predicted SCFA-related fermentation pathway and cell wall/PAMP-related pathway.Host-independent data provide cellular and transcriptome-level context for testing the three-level "biota-function-host" hypothesis.

Conclusion

Treatment pathways should serve as the primary comparison frame.The acetate/SCFA axis and cell wall/PAMP axis, together with the mTORC2-RhoA-NLRP3 host context, are testable hypotheses rather than proven mechanisms.

Keywords: gastric cancer; 16S rRNA; treatment pathway-related microbiome remodeling; chemoradiotherapy combined with immunotherapy; chemotherapy immunotherapy; pathological complete response; PICRUSt2; pharmacogenomics

1.Introduction

Gastric cancer is one of the common malignant tumors of the digestive system. [1, 2] For patients with locally advanced disease, perioperative or neoadjuvant comprehensive therapy is an important strategy, which can improve the tumor regression rate, increase the chance of surgery, and prolong survival. [3-7] In recent years, immune checkpoint inhibitors have been incorporated into the gastric cancer treatment system. [8-10] Therefore, chemotherapy combined with immunotherapy and "radiation therapy + chemotherapy + immunity" combined regimen have become clinically significant treatment models. [11-14] Pathological complete response (pCR) is a key endpoint to evaluate the sensitivity of neoadjuvant/perioperative treatment, but there is still significant heterogeneity in patient response to treatment under similar treatment backgrounds. [15, 16]

The microbiome may affect tumor treatment response through the host immune microenvironment, inflammatory response, oxidative stress, competition for nutritional sites, and treatment-related tissue damage.[17-21] Existing studies suggest that microbial-derived short-chain fatty acids, cell wall components, PAMP signals, and redox status can regulate host immune responses.[22-24] In patients receiving radiotherapy, chemotherapy, and immunotherapy, treatment pressure may reshape the local tissue environment and microbial ecological status.[25, 26] Different treatment pathways may also correspond to different microbial backgrounds.[15, 27-29] Therefore, when analyzing the relationship between microorganisms and pCR, treatment pathways should be stratified rather than simply combining all samples.

However, 16S rRNA amplicon sequencing mainly reflects microbial composition.[30, 31] It cannot directly demonstrate metabolite changes, functional gene activity, host signaling pathway activation, or cell death mechanisms.[32, 33] Therefore, a clear boundary of evidence must be maintained between "differences in

microbial composition" and "predicted function of PICRUSt2" and "host mechanism hypothesis". [34] The latest research on inflammatory cell death and destructive death of mitochondrial oxidative membranes suggests that innate immune activation and insufficient nutrient supply may jointly promote mitochondrial ROS, membrane oxidative damage, and NLRP3 inflammasome-related reactions.[35, 36] The mTORC2-RhoA axis may be involved in the host inflammatory program. [37] This study only uses this mechanism framework as a future host verification direction; it cannot be proven based on 16S data alone. [38]

Based on 91 post-treatment gastric cancer samples, we used RCI versus CI as the main comparison, and performed separate pCR analysis within each treatment path.We integrated OTU-level community distance and genus-level CLR-limma models to explicitly test treatment × response interactions and examine the overlap between treatment-related genera and RCI response-related genera.PICRUSt2 was then used to define the functional directions of candidate acetate/SCFA and cell wall/PAMP, and external host background analysis and GDSC2 compound priority screening were carried out.Since the cohort lacks pre-treatment samples, matched metabolomes, and host experiments in the same cohort, the endpoint is positioned as "ecological and mechanistic hypotheses related to treatment pathways" rather than proof of "microbial changes caused by radiotherapy" (Figure 1).

Research design and hierarchy of evidence.

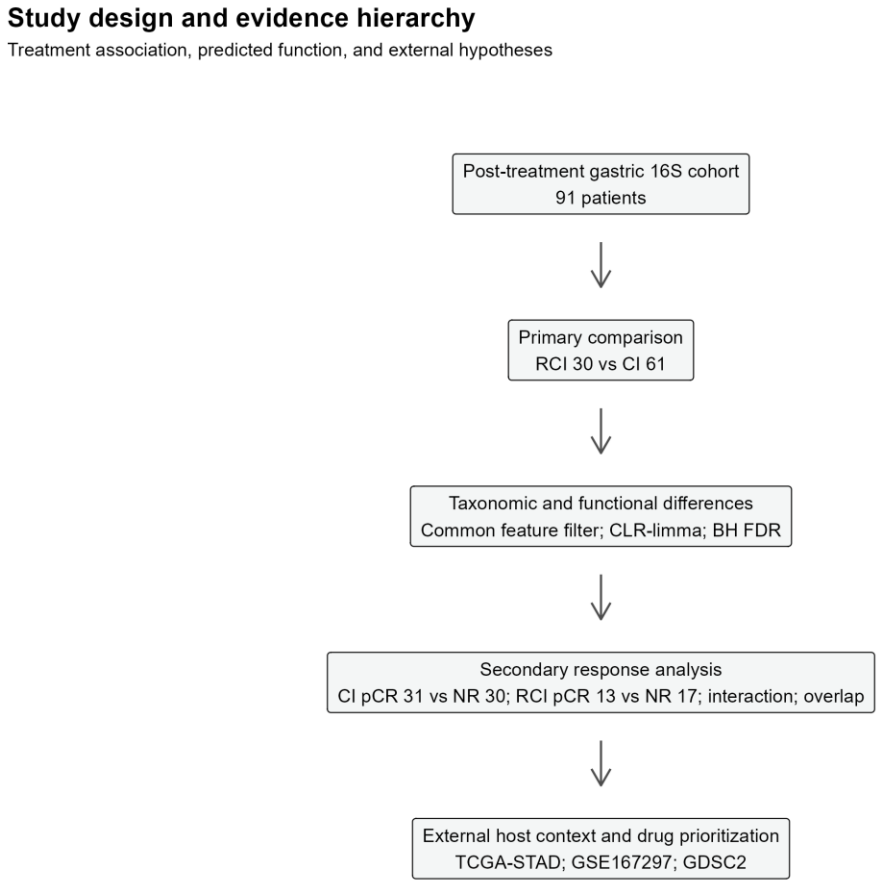


Figure 1. Our first step is to first compare the post-treatment cohort by treatment pathway (RCI vs CI).The second step is to conduct secondary reaction analysis in CI-pCR vs CI-NR and RCI-pCR vs RCI-NR, and conduct predictive function, external host background and in vitro drug priority screening.

2. Methods

2.1 Study Subjects and Grouping

2.1 Research objects and groupings

The cohort included 91 gastric cancer samples with 16S rRNA sequencing data.According to the treatment plan, it was divided into CI (n=61) and RCI (n=30).TRG0 was defined as pCR, and TRG1–3 were defined as non-pCR.Four treatment × response subgroups were formed: CI-pCR (n=31), CI-non-pCR (n=30), RCI-pCR (n=13), RCI-non-pCR (n=17).[39-41] All results are interpreted as correlations with treatment-conditioned microbial status or response in existing samples.

2.2 16S rRNA data source and quality audit

The original 16S rRNA amplicon data of this study was saved in paired-end FASTQ. [42, 43] The original FASTQ list indicated that a total of 91 cases entered downstream analysis.There are also 10 suspected DNA_CK and PCR_CK control files.

Workflow statistics show that there are 91 16S samples in this study. [44, 45] The original number of reads was 12,496,103, and the number of valid reads after quality control and merging was 10,015,083, with a retention rate of approximately 80.1%.The range of valid reads per case is 74,199–195,574, the number of digits is 102,602, and the mean is 110,055.9.

Downstream analysis uses taxonomic abundance tables, α/β diversity results, differential analysis results, and PICRUSt2 functional prediction results.OTU-level Bray-Curtis distance matrices were used for main therapeutic pathway beta diversity comparisons; genus-level abundance tables were used for constitutive taxonomy and pathway modeling[46-48].

2.3 Diversity analysis

Chao, Sobs, Shannon and Simpson indices were used for alpha diversity.Comparisons between groups were performed using the Wilcoxon rank sum test with Benjamini-Hochberg correction within preset comparison families.Beta diversity uses the OTU-level Bray-Curtis distance matrix for the main analysis of CI by RCI (because the original OTU distance cannot be reproduced after aggregation to the genus level).Visualization uses PCoA.PERMANOVA was used as the main reference, and independent 9999 replacement R recalculations, depth-corrected marginal PERMANOVA and betadisper sensitivity analysis were conducted.[49-52]

2.3.1 Four groups of layers overlap with ellipses

To maintain treatment-specific interpretation, CI and RCI are each divided into CI-pCR, CI-NR, RCI-pCR and RCI-NR according to pathological response.The global Kruskal-Wallis test was performed first, followed by all pairwise Wilcoxon tests with multiple correction.In Figure 2D, the 95% confidence ellipse is estimated for the first two PCoA coordinates of the Bray-Curtis matrix; the polygon intersection and IoU are calculated geometrically.Ellipse overlap is shown for descriptive purposes only and not as a test of inference[53-56].

2.4 Analysis of differential bacteria and composition robustness

Bacteria with differences at the genus level were screened through exploratory Mann-Whitney test and CLR-limma model.Multiple corrections were performed on the complete set of candidate features in the control.LEfSe results from the process are used for candidate visualization.In CLR-limma, non-target features are removed, filtered by abundance occurrence rate and mean, pseudo-counts are added and central log ratio transformation is performed.The Limma model incorporates log sequencing depth as a covariate.The model form is:

CLR(genus) ~ group + log_reads.This analysis was used to assess directional robustness and candidate prioritization screening and was not used to define clinical biomarkers individually[57-60].

2.4.1 Exploratory LDA priority screening

For eligible bacterial genera, the univariate LDA pattern score of the square root of the between-group variance/within-group variance ratio was calculated as log10 relative abundance. Sort bacterial genera according to four groups of comparisons; The 8 features with the highest scores enter MASS: : lda,generates normalized projections for visualization. This analysis was not cross-validated and does not serve as a clinical classifier[61-64].

2.4.2 Candidate pathway connection

The top 20 features of four groups of LDA were taken, and after deduplication, there were 19 bacterial genera. For Exiguobacterium, all tag lines were first summarized at the genus level and then abundance statistics and pathway connections were performed. CENTFERM-PWY is classified as a SCFA-related fermentation pathway (pyruvate fermentation to butyrate) according to the annotation, and is not interpreted as direct acetate production. The host characteristics of TCGA-STAD and GSE167297 were analyzed independently and were not matched with the microbial sample IDs one by one. This connection is exploratory and does not infer metabolite concentrations or pathway activity.

To transparently disclose the genus level results, we report control and treatment group labels, median abundance, detection rate of both groups, descriptive log2 change and 95% confidence interval, depth-corrected q value, direction and stability under 9 pseudo-count/abundance thresholds in the supplementary table. The combined detection rate field gives two sets of percentages; The q value is displayed in scientific notation or $q<0.01$[65-69].

2.5 Treatment Path × Response Interaction Model

To evaluate whether the relationship between microbial characteristics and pathological response changes with treatment path, we fit an exploratory interaction model for all 91 cases:

Horizontal features are first filtered by occurrence rate and mean, and then CLR transformed. The interaction term was used to test whether the treatment path modified the relationship between bacterial flora and pCR. All interaction results are subject to multiple corrections and are for exploratory interpretation only[70-73].

2.6 RCI clinical data matching

To determine whether response-related signals in RCI subgroups were affected by imbalances in available clinical variables, we performed matching and quality control on additional RCI clinical tables. Used hospitalization number as the primary key and name as the auxiliary key to match 91 cases in the 16S queue. Only existing RCI samples in the 16S cohort were used for clinical covariate screening; Unmatched samples did not enter microbiological analysis. The Wilcoxon rank sum test was used for continuous variables and the Fisher exact test was used for categorical variables between RCI-pCR and RCI-NR, and multiple corrections were made.[74-77]

2.7 PICRUSt2 function prediction and host hypothesis

PICRUSt2 is used to predict microbial functional potential from 16S lineage inference. Two types of directions are prespecified: Acetate/SCFA-related fermentation and cell wall/PAMP-related synthesis. SCFA candidate pathways include MetaCyc pathways containing acetate or butyrate products in the annotations, such as P163-PWY, P461-PWY, PWY-5100, PWY-5676, and PWY-5677. Cell wall/PAMP candidates include wall phosphate/teichoic-acid, peptidoglycan, lipopolysaccharide, and lipid A-related pathways. METH-ACETATE-PWY is not used for the explanation of acetic acid generation because it is annotated as a methanogenesis process involving the acetic acid product (consuming acetic acid). PICRUSt2 results are considered "predictive potential" only and not measured metabolic activity or metabolite concentrations.

External resources are used to assess biological feasibility and screen and validate targets: Functional pathways, metabolites, host genes and microbial immunological information serve as supporting evidence. The outer layer does not demonstrate changes in metabolites or host pathways in the current cohort. The mTORC2-RhoA-NLRP3 axis is associated with cell wall/PAMP and immunometabolic cues under the framework of "host-side hypothesis to be verified"[34, 78, 79].

2.8 External public gastric cancer organization benchmarks

For directional comparison with independent tissue controls, we downloaded the supplementary table of the public gastric cancer mucosal dataset PRJNA532731. The table contains 123 cases, including 61 pairs of numerically matched cancer/non-cancerous tissues. Shannon diversity, number of observed OTUs and Chao1 were compared respectively, and paired IDs were compared using the paired Wilcoxon test; Bray-Curtis PCoA and unpaired and paired stratified PERMANOVA were used at the community level. Overlay the published differential bacteria with the current pre-screened collection for directional consistency reference.

2.9 Multi-omics analysis

Within RCI, we calculated Spearman correlations between the top 6 treatment-relevant genera and the top 6 RCI-responsive candidate genera and the preset MetaCyc pathway set. This related analysis is based on the same 16S input and is only used for internal consistency assessment and does not constitute independent verification. The public TCGA-STAD PanCancer Atlas RNA-seq is used to calculate host signatures (mTORC2, RhoA signaling, NLRP3 inflammasome, macrophage status, CD8 cytotoxicity, IFNG response, T cell exhaustion, antigen presentation) and remove shared genes before correlation analysis to reduce cyclic dependence.

2.10 External single-cell, bulk transcriptome and pharmacogenomic virtual screening

To translate the "biota-function-host" hypothesis into testable candidates, we performed an in vivo deductive intervention and target-matched drug prioritization analysis. Default host modules include SCFA receptor and HDAC regulation, PAMP sensing, mTORC2-RhoA signaling, inflammasome/IL-1 activation, antigen/IFN response, macrophage and T cell status. Download GSE167297 single-cell RNA-seq and locate the above modules to mark inferred cellular compartments; This analysis used a partitioning and patient balancing strategy and is not a direct validation of the current cohort.

Pharmacogenomics prioritization uses GDSC2 dose-response tables and Cell Model Passports metadata (from GDSC/Sanger). Gastric cancer and STAD cell lines were retained. Drugs whose direct targets are in the mTOR/PI3K/AKT, ROCK, HDAC or PAMP-inflammatory category are sorted by the median Z value of available STAD cell lines, and the number of cell lines and the proportion of Z<-0.5 are given. This ranking represents an in vitro probe screen, is not a clinical treatment recommendation, and does not model immune-microbial co-culture.

In external single cell analysis, first read the GSE167297 raw count matrix in sparse format: Cells with nFeature 200–7500, nCount≥500, and mitochondrial content ≤20% are retained. Subpopulation annotation including epithelial, myeloid/macrophages, T/NK, B/plasma cells, fibroblasts/stromal, endothelial and mast cells were performed by marker inference. Tumor versus normal comparisons were aggregated at the patient level, and paired tests were performed only on patients with dual compartments. CellChat was run on a balanced subset of up to 250 cells per annotation type (1,750 cells total, 7 classes) using CellChatDB.human and employing 25 bootstraps with censored mean estimates. Slingshot performs pseudo-time series on epithelial cells in UMAP space, with normal rich clusters as the starting state. CellChat and pseudochronology are exploratory and are not to be interpreted as treatment-specific or chronological evidence.

2.11 Statistical analysis

Descriptive statistics using distribution matching were used for continuous variables; Alpha diversity was corrected using Wilcoxon rank sum + BH; Beta diversity combined, OTU-level PERMANOVA, independent permutation recalculation, depth-corrected marginal PERMANOVA, ANOSIM and betadisper when available. Taxonomy and pathway comparison were performed using CLR-limma with sequencing depth and multiplex correction. Findings without multiple correction but with directional nominal trends were recorded as exploratory. The treatment × response intersection is defined as: Under strict effect filtering and nominal direction filtering, the same bacterial genus satisfies both the positive correlation with treatment and the positive correlation with RCI response. Drug prioritization was summarized descriptively by direct target matching and GDSC2 STAD sensitivity.

3.Results

3.1 Queue composition and sequencing quality

This cohort includes 91 post-treatment gastric cancer 16S samples: 61 cases were CI and 30 cases were RCI. TRG0 was defined as pCR (44 cases), and TRG1-3 was defined as non-pCR (47 cases). The four treatment × response subgroups were CI-pCR (n=31), CI-non-pCR (n=30), RCI-pCR (n=13), and RCI-non-pCR (n=17).

The sequencing process reported 12,496,103 original reads and 11,015,083 valid reads, with a retention rate of approximately 90.1%. The effective read range of each case is 74,199–195,574, with 102,602 digits.

3.2 RCI and CI have different treatment-related microbial statuses

In the main comparison, the Shannon index in RCI was lower than CI (mean 3.36 vs 3.74, p=0.034, q=5.06e-02); Simpson was also different (p=0.021, q=5.06e-02), while the difference in Chao richness was not significant (p=0.574, q=5.74e-01). The results suggest differences in abundance distribution within groups rather than significant changes in observed richness (Fig. 2A–C).

OTU-level Bray-Curtis analysis showed an overall slight difference between RCI and CI (PERMANOVA R2=0.0205, p=0.005). Independent 9999 replacement recalculations also yielded R2, p=0.0058; Depth-corrected marginal model R2=0.0220, p=0.0029. Betadisper has no dispersion difference (p=0.5889). The data therefore support small, treatment path-related community drift rather than a clean separation of the two communities (Fig. 2D).

In CLR-limma, Citrobacter is higher in RCI than CI (coefficient 1.513, p=3.42e-04, q=3.42e-02); RCI mean relative abundance is 0.00505, corresponding CI is 0.00116; The detection rates were 66.7% and 32.8% respectively. Bacteroides, Akkermansia, Lactococcus and Rhodococcus are nominally ranked bacterial genera in the next echelon, but their q values are all >0.05 after correction (Figure 2E-F).

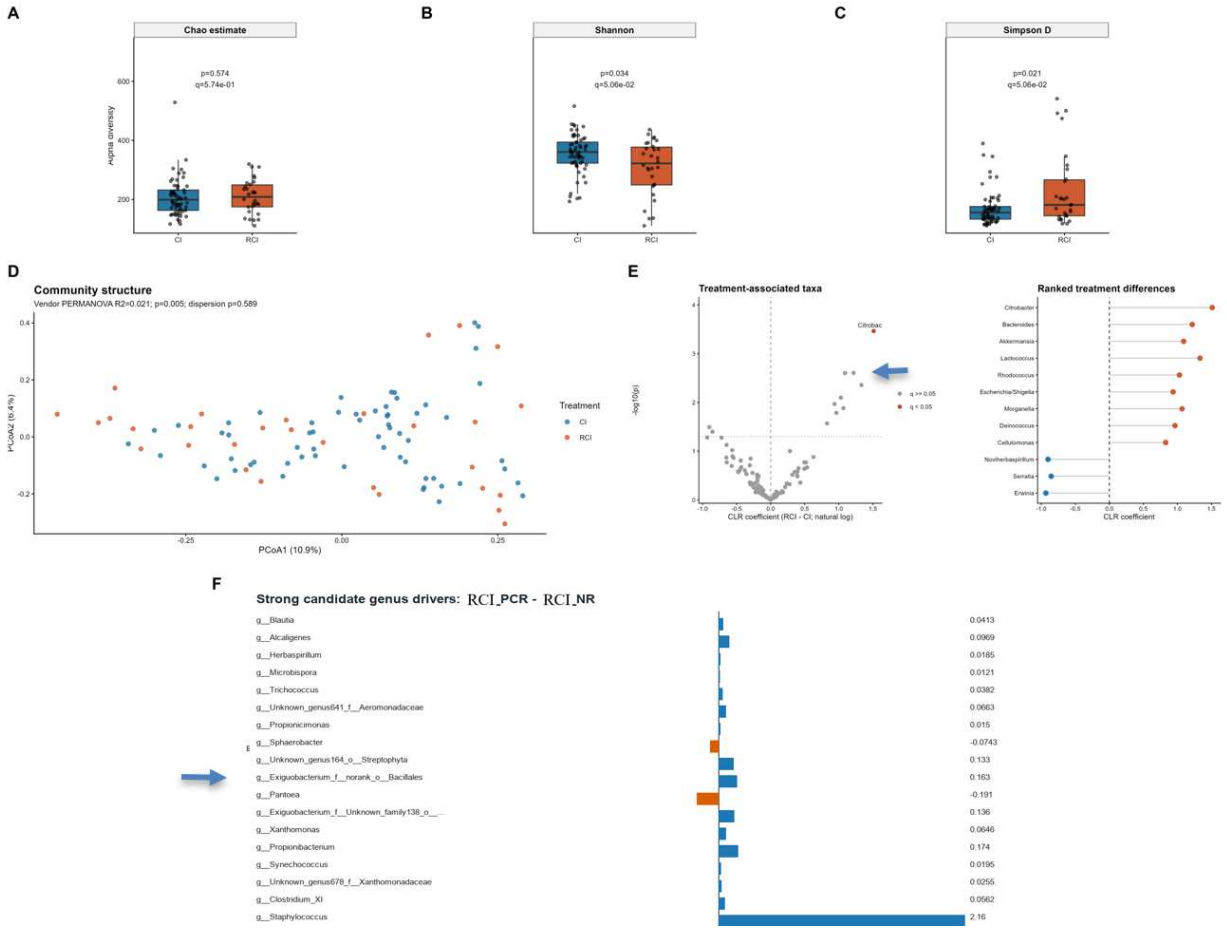


Figure 2. Treatment stratification ecology and treatment-related bacterial genera. A, Chao richness; B, Shannon index; C, Simpson index; D, Bray-Curtis PCoA and RCI/95% confidence ellipse and its geometric

intersection; E, Merged view of CLR-limma volcano plot with treatment coefficient ranking; F, Abundance RCI-PCR versus NR master comparison. The intersection and ranking of candidate bacterial genera are descriptive results.

3.3 Four-component stratification and exploratory LDA prioritize screening of candidate bacterial genera

In the comparison of four groups (CI/RCI × pCR/NR), Shannon (p=0.008, q=2.43e-02) and Simpson (p=0.029, q=4.31e-02) were still significant, while Chao richness was not significant (p=0.143, q=1.43e-01). The differences in pairwise comparisons after multiple correction were mainly concentrated in the controls involving RCI-NR: RCI-NR was lower than CI-NR and CI-pCR on Shannon (q<0.01), and the difference between RCI-NR and RCI-pCR was significant (q=3.04e-02). This model supports a treatment condition explanation rather than a pCR effect shared by both pathways. In the PCoA geometric diagram, the IoU between the 95% CI ellipse and the RCI ellipse is 0.53, indicating a shared community space; This geometric overlap does not replace the PERMANOVA test.

Among the four groups of feature priority screening, Lactococcus, Citrobacter, Staphylococcus, Erwinia, Pantoea and Bacteroides ranked at the top of the LDA style effect size (2.234, 2.107, 2.032, 1.988, 1.872, 1.844).

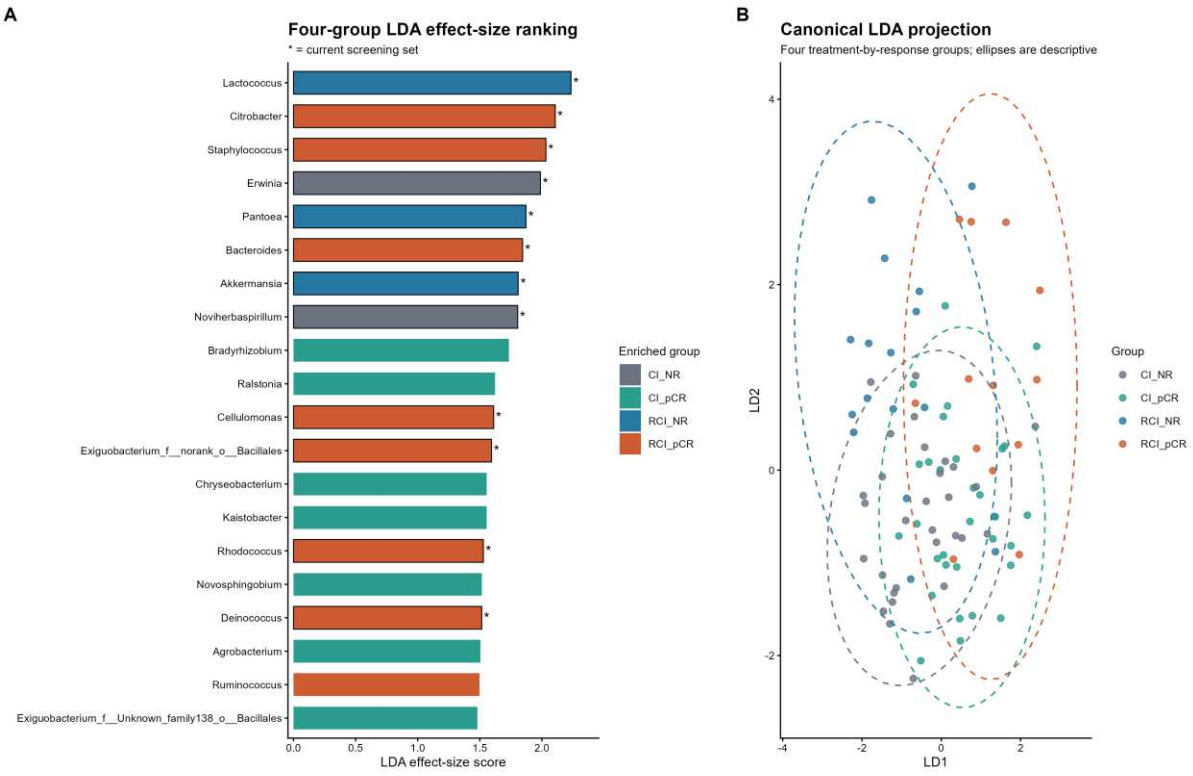


Figure 3. Four groups of LDA prioritization and orthogonal projection. A, Ranking of the top 20 bacterial genera by univariate LDA pattern isolation scores in four groups (CI-NR, CI-pCR, RCI-NR, RCI-pCR). B, eight-feature MASS: : Orthogonal projection of the lda model.

3.3.1 LDA priority bacterial genera

Because LDA effect size ranks 12th (1.594), is enriched in the RCI-pCR direction, and the median relative abundance in RCI-pCR is higher than that in RCI-NR (0.00288 vs 0; detected in 10/13 vs 3/17 cases), Exiguobacterium was selected as a representative low-exploration candidate for the radiotherapy response branch.

For Exiguobacterium, the existing PICRUSt2 table suggests that it is combined with CENTFERM-PWY (pyruvic acid fermentation to butyric acid), PWY-6397 (mycolyl-arabinogalactan-peptidoglycan complexcompound biosynthesis), PWY-5265 (staphylococcal peptidoglycan biosynthesis), KDO-NAGLIPASYN-PWY ((Kdo)2-lipid A biosynthesis), and P42-PWY (incompletely reduced TCA cycle), etc. have potential connections.

3.3.2 Exiguobacterium defines a testable three-layer microenvironment hypothesis

In order to avoid compressing the level of evidence, we decomposed the Exiguobacterium signal into three layers of "bacteria-function-host" for explanation. At the genus level, g__Exiguobacterium_f__norank_o__Bacillales ranked 12th (1.594) among the four groups of LDA scores and was enriched in the RCI-pCR direction; The four sets of global tests did not reach significance (q=4.16e-01). After summarizing all Exiguobacterium lines, the median relative abundance of RCI-pCR was 0.00288, RCI-NR was 0, and the detection rate was 10/13 vs 3/17. This signal is the reaction direction signal within the radiotherapy-related pathway. In the main comparison RCI vs CI, the median values are RCI 0 and CI 0.00148 respectively.

At the functional level, Exiguobacterium is connected to a SCFA-related fermentation pathway, CENTFERM-PWY (pyruvic acid fermentation to produce butyrate; rho=0.224, q=6.65e-01 in RCI) and multiple cell wall/PAMP related annotations (PWY-6397: rho=0.321, q=5.59e-01; PWY-5265: rho=0.303, q=5.98e-01; KDO-NAGLIPASYN-PWY: rho=-0.277, q=6.47e-01). The SCFA branch therefore represents predicted fermentation potential rather than measured acetate/butyrate production; The cell wall/PAMP branch represents predicted structural potential rather than ligand exposure or TLR/NOD/NLRP3 activation. At the host level, independent TCGA-STAD signatures showed synergistic relationships between CD8-IFNG (rho=0.852, q<0.01), antigen presentation-NLRP3 (rho=0.590, q<0.01), NLRP3-RhoA (rho=0.312, q<0.01), and RhoA-mTORC2 (rho=0.218, q<0.01). GSE167297 places PAMP/inflammasome signals in similar myeloid compartments, antigen/IFN/cytotoxic signals in T/NK and myeloid compartments, and CellChat shows extensive MHC-I/MHC-II communication. Three levels of data support the stratification hypothesis: The Exiguobacterium signal in the RCI-pCR direction may represent a community with both SCFA fermentation and cell wall/PAMP potential, and may interact with myeloid innate recognition and T/NK antigen-IFN status.

Figure 4. Exiguobacterium candidate prioritization and prediction function connection. A, Query boundary PubMed count of LDA-preferred bacterial genera; B, Covariation of low-exploring genera within RCI with pathways selected by PICRUSt2, highlighting the main candidate Exiguobacterium. This figure shows literature and predicted mapping and does not represent evidence of novelty, metabolite production, or pathway activation.

3.4 External gastric tissue benchmark shows differences in cancer tissue and non-cancerous tissue communities

Next, we examine whether the current candidate framework is consistent with the direction of the independent gastric mucosa "cancerous tissue vs. non-cancerous tissue" control. Among the 61 paired samples in PRJNA532731, the mean Shannon value of tumor tissue was significantly higher than that of non-tumor (1.442 vs 1.114, p=3.31e-03, q<0.01), the observed OTU richness was higher (240.1 vs 129.7, p=5.05e-07, q<0.01), and the Chao1 was higher (301.9 vs171.5, p=2.54e-06, q<0.01). However, community-level segregation is not robust to permutation tests in this benchmark (unpaired PERMANOVA R2=0.0174, p=0.0679; Paired stratified PERMANOVA R2=0.0174, p=0.0949).

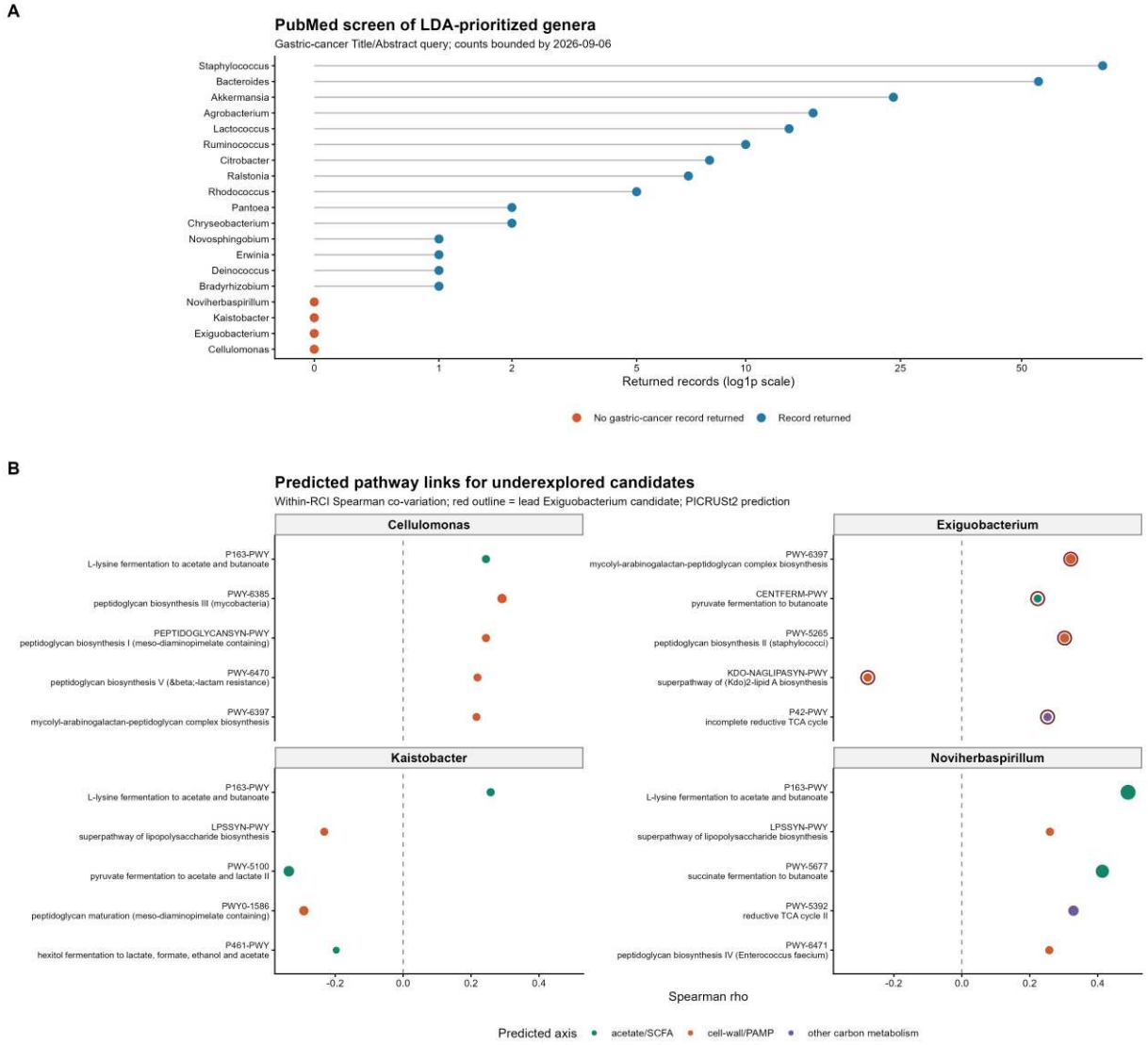


Figure 5. Independent gastric cancer and non-cancerous tissue benchmarks. A, Comparison of pairwise alpha diversity of 61 paired samples of PRJNA532731; B, Bray-Curtis PCoA and unpaired and paired stratified permutation statistics; C,

Visualization of the intersection of disclosed differential bacteria and the current screening set, Bacteroides is an overlapping genus.

3.5 Separate evaluation of reaction-related signals in CI and RCI

No difference in alpha diversity was found between pCR and non-pCR within CI; Shannon mean value is 3.77 vs 3.71 (p=0.756, q=9.48e-01), Simpson and Chao are also not significant.

Within RCI, Shannon in the pCR group was higher than that in the non-pCR group (3.69 vs 3.10, p=0.015, q=4.56e-02); Chao richness also increased numerically (237.62 vs 188.82, p=0.038, q=5.42e-02), and Simpson was close to the boundary (p=0.054, q=5.42e-02). RCI response β diversity did not reach significance, indicating that the response signal was mainly α diversity mode.

3.6 Response-related bacterial genera have therapeutic specificity and exploratory characteristics

CLR-limma protobacteria within RCI include Gluconacetobacter (coefficient -1.887, p=0.0052), Pantoea (-1.935, p=0.0082) and Staphylococcus (0.982, p=0.012); None of them passed multiple corrections, and Staphylococcus was retained as an exploration candidate because of its positive directionality in the RCI-pCR direction.

Within CI, Lactococcus was lower in pCR than non-pCR (CLR-limma coefficient=-1.836, p=2.39e-04, q=2.39e-02). Since the α and β comparisons of CI were not significant and their treatment backgrounds were different, this finding only served as a CI-specific exploration signal and was not combined with RCI candidates.

3.7 PICRUSt2 defines candidate acetate/SCFA and cell wall/PAMP functional directions

After defining therapeutically relevant ecological differences, we used PICRUSt2 to convert the 16S lineage into MetaCyc functional potential, focusing on acetate/SCFA-related fermentation and cell wall/PAMP-related synthesis. This step is only for generating testable metabolic and immune hypotheses and is not intended to demonstrate measured metabolic changes or pathway activation.

None of the 422 qualified MetaCyc pathways in the RCI-vs-CI comparison passed multiple calibration. Among the preset candidates, P163-PWY (lysine fermentation produces acetic acid/butyric acid) SCFA direction coefficient is the largest (1.812, p=0.0159, q=8.18e-01); The LPSSYN-PWY (lipopolysaccharide biosynthetic superpathway) cell wall/PAMP correlation coefficient is positive (1.389, p=0.0879, q=8.18e-01); The TEICHOICACID-PWY difference is not significant (0.141, p=0.306, q=8.18e-01). These are ranking clues rather than statistical corroboration of changes.

The complete list of candidate pathways (including ID, definition, coefficient, p/q value and evidence boundary) can be found in the CSV source data.

Within the RCI, 9 of the 204 preset bacterial genus-pathway pairs still retained strong correlations through subsequent multiple corrections: Includes Staphylococcus–PWY-5265 (peptidoglycan biosynthesis; rho=0.910, q<0.01), Proteus–KDO-NAGLIPASYN-PWY (lipid A biosynthesis; rho=0.703, q<0.01),

Rhodococcus–PWY-6397 (cell wall complex biosynthesis; rho=0.684, q<0.01), Lactococcus–PWY-5677 (succinic acid is fermented to produce butyric acid; rho=0.632, q<0.01), Lactococcus–PWY-5100 (pyruvic acid is fermented to produce acetic acid and lactic acid; rho=0.606, q=1.59e-02). The correlation between Citrobacter and P461-PWY (rho=0.442, p=0.0146, q=1.24e-01) and P163-PWY (rho=0.364, p=0.0481, q=2.18e-01) is only nominal and has not passed the correction. Since the bacterial genus and pathway come from the same 16S input, this network is more of an internal consistency analysis and not an independent verification.

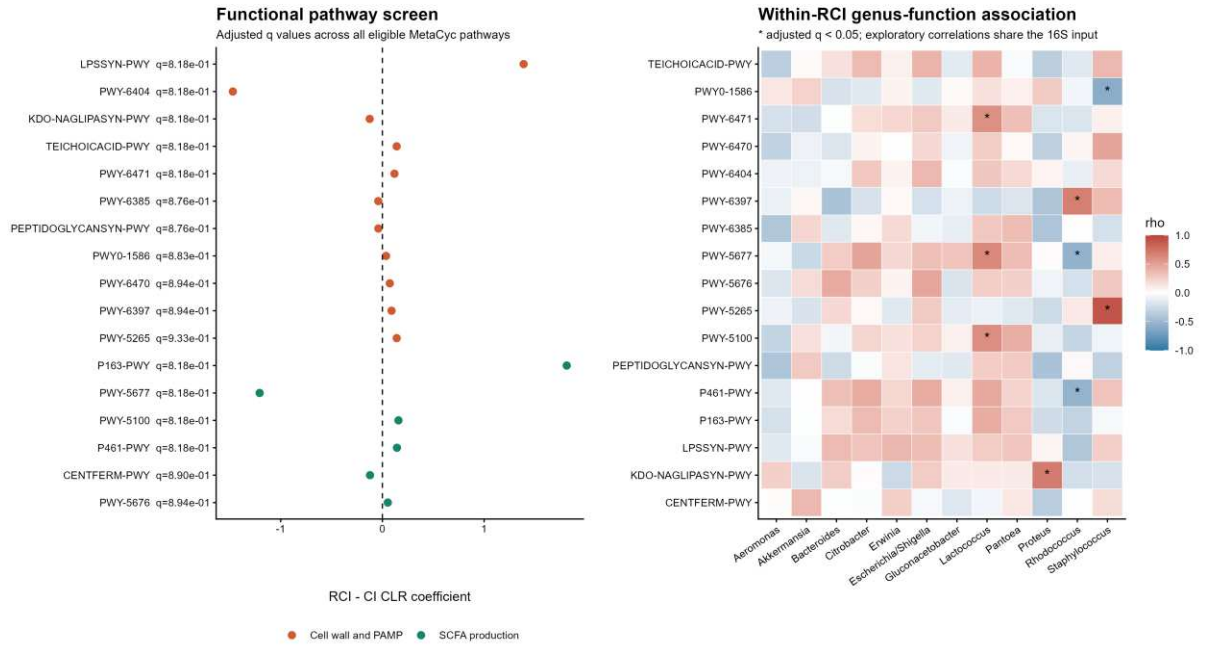


Figure 6. Predicted functional candidates and microbiota-pathway associations within RCI. A, Preset MetaCyc direction in treatment comparison; B, Exploratory microbiota-pathway covariation within RCI. PICRUSt2 features represent predictive potential and internal traceability.

3.8 External host data support testable immune axis hypothesis

The predicted functional direction is used to propose a host-side verification framework rather than a direct proof. The proposed mTORC2-RhoA-NLRP3 connection links cell wall/PAMP sensing and immunometabolic stress to innate immune and inflammasome responses.

TCGA-STAD blocks are used to evaluate preset immune signature relationships, after removing shared genes; GSE167297 single-cell observation of the distribution of the same module within the marker inference compartment. This analysis determines whether candidate host modules form a reasonable and interpretable immune environment for gastric cancer.

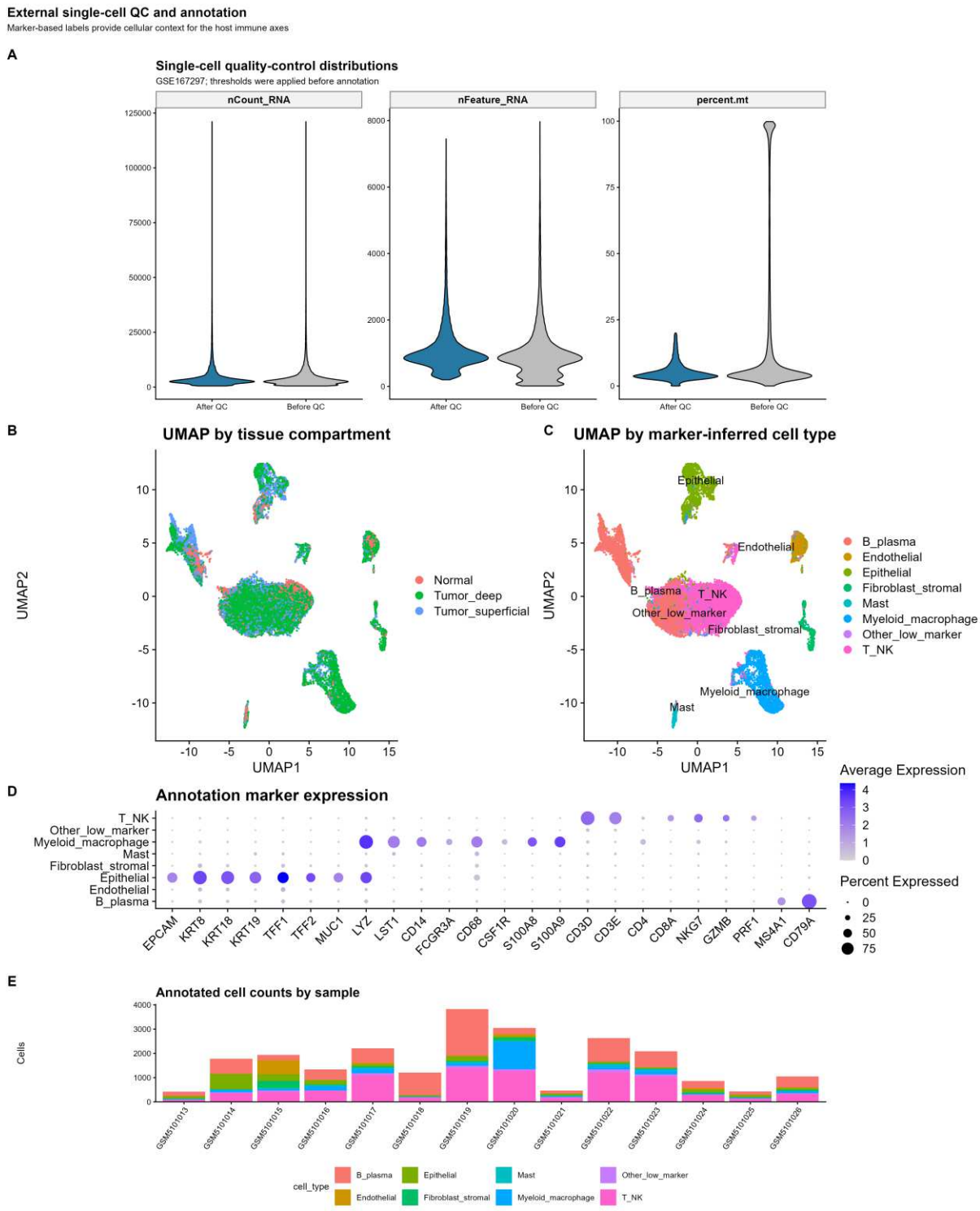
Among 412 cases of TCGA-STAD tumors, CD8 cytotoxicity was strongly correlated with IFNG response (rho=0.852, q<0.01); NLRP3 inflammasome is also associated with IFNG response (rho=0.652, q<0.01),

antigen presentation (rho=0.590, q<0.01) and macrophage-related signatures; The correlation between mTORC2 and RhoA signal is positive (rho=0.218, q<0.01).

Among external single cells, the marker-inferred myeloid/macrophage population scored higher on the PAMP sensing and inflammasome-IL-1 modules than the T/NK population; The antigen/IFN/cytotoxicity score was more prominent in the T/NK and myeloid groups.

3.9.1 Single-cell quality control and label inference annotation

There were 30,365 cells before GSE167297 data quality control, and 23,310 cells (76.8%) were retained according to the threshold. After quality control, the median nCount increased from 2,971 to 3,023, nFeature increased from 850 to 941, and the mitochondrial proportion decreased from 5.20% to 4.35%. The inferred markers identified 8,405 T/NK, 7,788 B/plasma cells, 2,177 myeloid/macrophage, 2,073 epithelial, 890 endothelial, 766 fibroblast/stromal, 496 mast cells, and 715 low markers. The UMAP compartment structure and labeling scores are shown in Figure 7



390

391 Figure 7. External single-cell quality control and marker inference annotation. A: Library size, detection
392 characteristics and mitochondrial content distribution before and after quality control; B: UMAP by tissue
393 compartment and inferred cell type; C–E: Marker modules, marker expression and cell type counting. Marked
394 as inferred results, for external reference only.

3.9.2 Comparison of normal-tumor modules for patient balance

There were 5 patients in the external cohort, 4 of whom had normal and tumor paired compartments, so the patient balanced paired test was based on 4 cases. None of the 42 "cell type × module" tests were significant after multiple correction (minimum q=2.34e-01). Myeloid/macrophages had descriptive increases in PAMP sensing (0.168 vs 0.083), inflammasome/IL-1 (0.488 vs 0.303), and antigen/IFN/cytotoxicity (1.163 vs 0.853) in the tumor compartment, but the paired differences in this small sample were not robust enough. This limitation is shown in the supporting source data sheet and Figure 7.

3.9.3 Exploratory epithelial pseudochronology

Apply Slingshot on 2,073 marker-inferred epithelial cells. The quasi-chronological series obtains the finite value of 257 cells: The median of normal cells was 0.007, that of tumor surface was 0.184, and that of deep tumor was 0.750. This trajectory places normally enriched cells at the lower end, with tumor-associated compartments continuing along higher states. (Figure 9A-C).

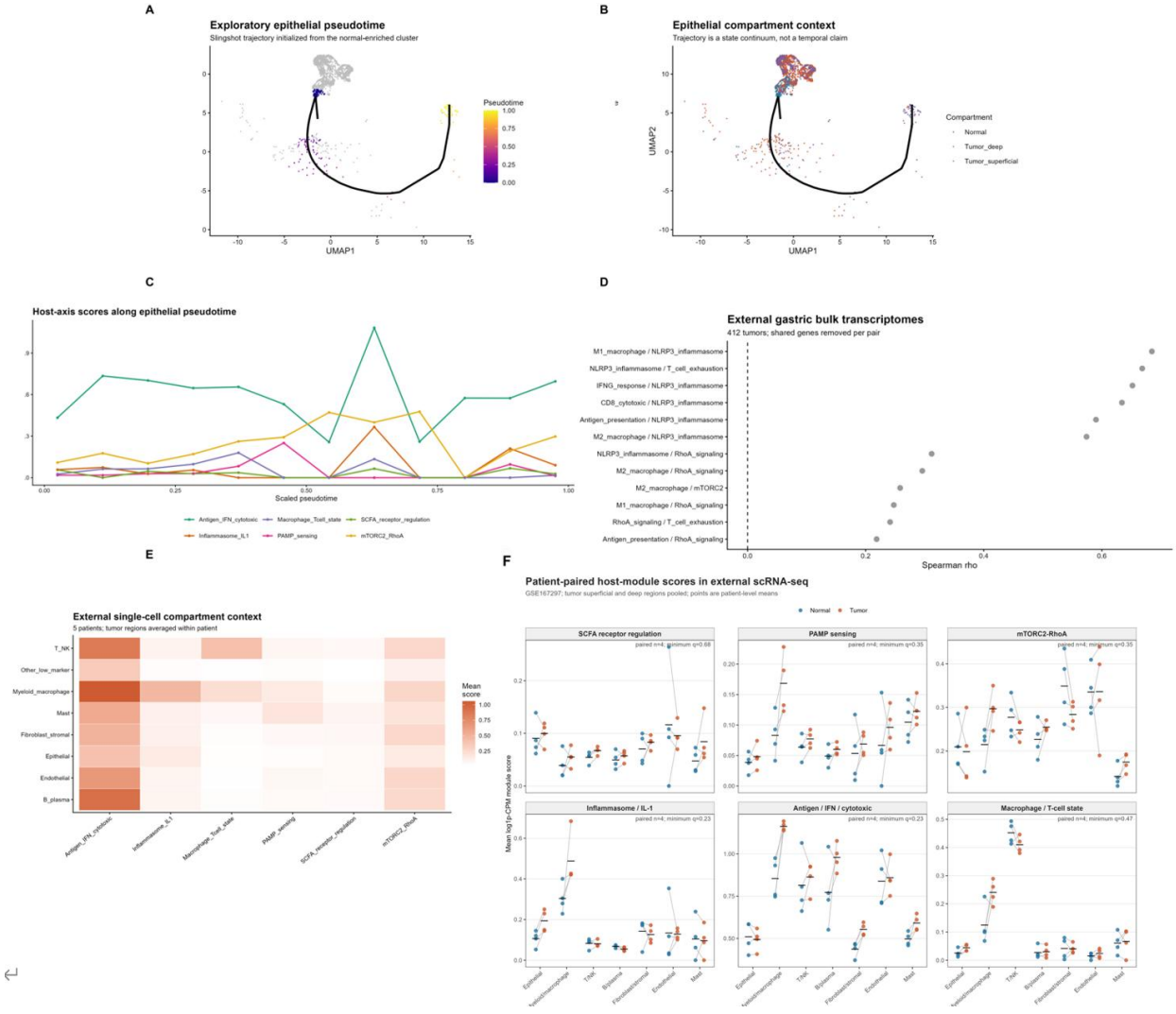


Figure 8. Analysis of external epithelial status and host context. A. Expression state quasi-sequential UMAP; B, Superposition of epithelial compartments; C, Host axis module score along the inferred continuity axis; D, TCGA-STAD volume signature correlation; E, Patient-balanced single-cell compartment context; F, Patient-balanced normal-tumor host module comparison. All are external data and descriptive results, not directly linked to current microbial samples or treatment pathways.

Combined with external data, the host end point of the Exiguobacterium hypothesis can be formed: Myeloid cells provide the PAMP/inflammasome background, and T/NK and myeloid cells provide the antigen/IFN/cytotoxic background. (Figure 9D-F).

In order to make the hypothesis feasible, we constructed a knowledge-driven annotation map: Map candidate bacterial genera and predicted pathways to candidate metabolites, receptors and host genes. Mapping sources include MetaCyc/PICRUSt2, KEGG, gutMGene, VMH/AGORA, CIDB and public host pathway knowledge.

The annotation path connects Exiguobacterium-associated SCFA fermentation candidates in the butyrate-prone direction, while placing their peptidoglycan and lipid A annotations into the cell wall/PAMP branch. The above predicted features further serve as testable host hypotheses connected to SCFA regulation, TLR2/NOD2, NLRP3-CASP1, IL1B/IL18 and mTORC2-RhoA modules. This map is a hierarchical annotation framework and is not direct evidence that Exiguobacterium produces metabolites in the current cohort or activates the host nodes mentioned above.

3.10 External single cell background and GDSC2 drug priority for experimental probe sorting

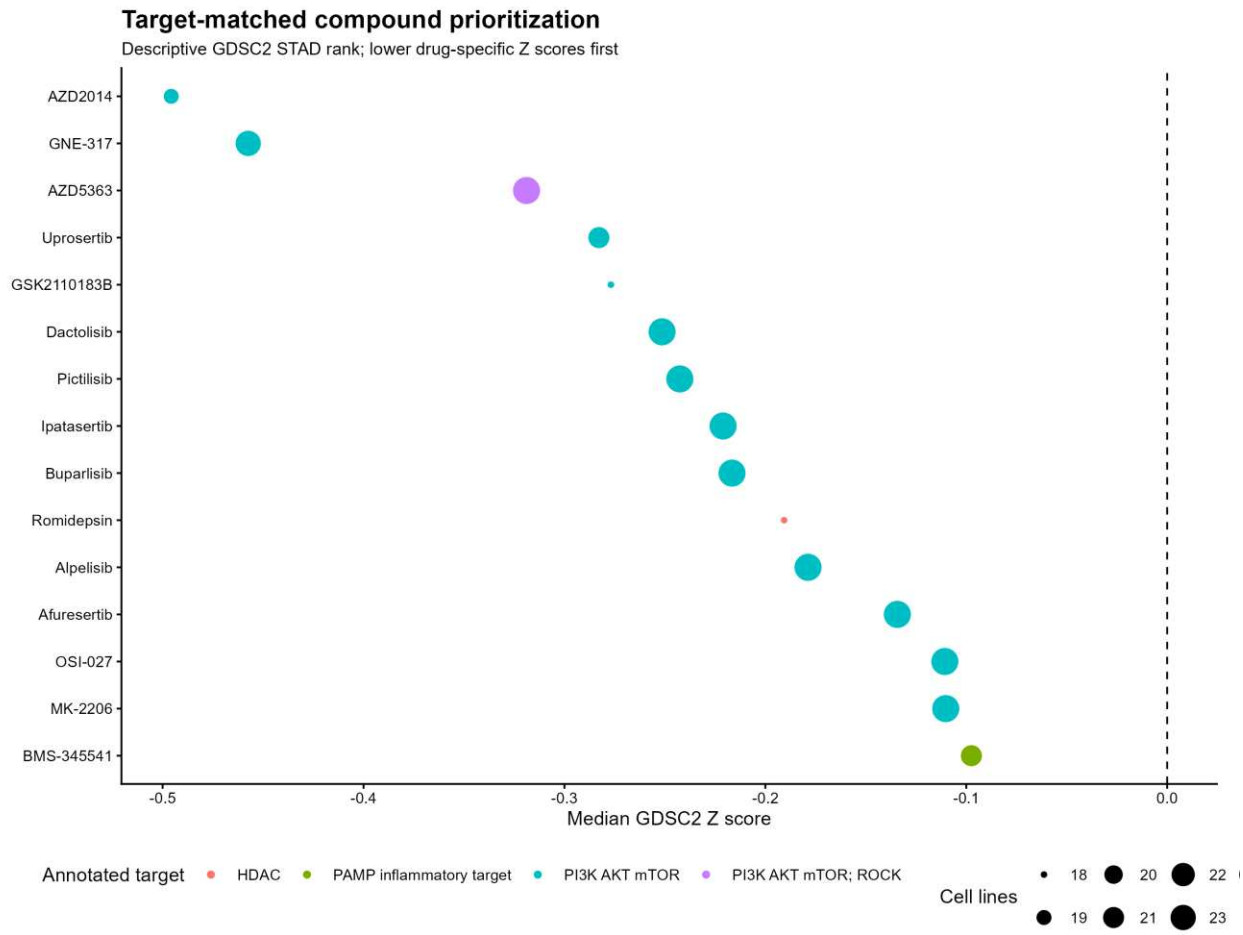


Figure 9. Direct target matching compound prioritization for GDSC2 STAD cell lines. The dot position indicates the median drug-specific Z value, the dot size indicates the number of STAD cell lines, and the color indicates the target category. This ranking is for experimental probe screening and is not a clinical recommendation.

External single-cell analysis localized candidate inflammatory and antigen/IFN modules to likely immune compartments but did not give drug response measurements, so GDSC2 served only as an experimental probe layer. Among the downloaded STAD records, 31 compounds had direct matching targets, covering 24 independent gastric/STAD cell lines.

The top targets are AZD2014 (mTORC1/mTORC2), GNE-317 (PI3Kalpha), AZD5363 (AKT/ROCK2), Uprosertib (AKT) and GSK2110183B (AKT); The median Z value of AZD2014 in 19 cell lines was -0.496, and 42.1% were lower than -0.5. These values describe tumor cell activity in GDSC2 and do not represent immune modulation, microbial dependence, radiotherapy interaction, or clinical benefit.

Therefore, this compound ranking should be understood as a list of experimental probes for mTOR/PI3K/AKT, ROCK, HDAC, and PAMP-inflammatory target categories, not a treatment

recommendation. Complete rankings, cell line results, target annotations and source information are provided with the analysis package.

Rank	Compound	Annotated target	Target class	Median GDSC2 Z	STAD lines	Fraction Z < -0.5
1	AZD2014	mTORC1, mTORC2	PI3K AKT mTOR	-0.496	19	0.421
2	GNE-317	PI3Kalpha	PI3K AKT mTOR	-0.457	23	0.478
3	AZD5363	AKT1, AKT2, AKT3, ROCK2	PI3K AKT mTOR; ROCK	-0.319	24	0.333
4	Uprosertib	AKT1, AKT2, AKT3	PI3K AKT mTOR	-0.283	21	0.476
5	GSK2110183B	AKT1, AKT2, AKT3	PI3K AKT mTOR	-0.277	18	0.389
6	Dactolisib	PI3K (class 1), MTORC1, MTORC2	PI3K AKT mTOR	-0.251	24	0.292
7	Pictilisib	PI3K (class 1)	PI3K AKT mTOR	-0.243	24	0.333
8	Ipatasertib	AKT1, AKT, AKT3	PI3K AKT mTOR	-0.221	24	0.417
9	Buparlisib	PI3Kalpha, PI3Kdelta, PI3Kbeta, PI3Kgamma	PI3K AKT mTOR	-0.217	24	0.375
10	Romidepsin	HDAC1, HDAC2, HDAC3, HDAC8	HDAC	-0.191	18	0.389

Table 1. Ranking of GDSC2 STAD compounds with direct target matching. The ranking is a descriptive median Z-score indicator and does not represent clinical efficacy or safety.

4. Discussion

This study is organized overall around "treatment pathways" rather than pCR alone. The primary comparison was RCI vs CI in 91 patients after treatment. The main result was a small but reproducible treatment-related shift in OTU-level community structure, accompanied by differences in alpha diversity distribution associated with Citrobacter's CLR-limma. [80]This signal defines the ecological context for interpretation of the response signal, but does not account for changes caused by radiation therapy alone due to the lack of pre-treatment samples and random assignment .

The community effect is small (R2=0.0205) and not driven by dispersion (p=0.5889). Independent 9999 permutation analysis yielded p=0.0058, and depth-adjusted marginal PERMANOVA yielded R2=0.0220 and p=0.0029. The combined results support small effects related to the treatment pathway rather than an overall replacement of the two communities.[23]

Reaction analysis is performed in separate ways. RCI-pCR sample Shannon was higher, but no RCI species were significant after multiple correction; Staphylococcus remains a candidate for directional exploration. Only Lactococcus in CI was associated with response after multiple correction. The results suggest that response signals may be treatment context dependent and should not be combined into "universal microbial biomarkers."

PICRUSt2 provides an entry point for functional interpretation, but its level of evidence is lower than that of measured metagenomes, transcriptomes, or metabolomes. The preselected acetate/SCFA and cell wall/PAMP pathways in the treatment comparison were not significant through correction, so P163-PWY, P461-PWY, PWY-5100, PWY-5676/5677, TEICHOICACID-PWY, peptidoglycan, LPS and lipid A were only used as candidate functional directions. [81]METH-ACETATE-PWY is excluded from the "acetic acid production" statement because it represents acetic acid consumption. This boundary setting is key to a believable flora-functional narrative.

The value of the mTORC2-RhoA-NLRP3 axis lies in providing a testable model on the host side rather than a purported mechanism. Publicly available TCGA-STAD data supports the synergistic relationship between NLRP3, macrophages, IFNG, antigen presentation, CD8 and RhoA-related signatures; External single-cell, CellChat, and trajectory analyzes place candidate signals into actionable cell and state context, but are not a substitute for cohort metabolomics, spatial transcriptomics, protein assays, or functional intervention[82].

The bacterial community-function correlation layer provides traceability between candidate bacterial genera and predicted pathways. Nine pairs in the RCI passed multiple corrections, including the cell wall/PAMP-related Staphylococcus-PWY-5265 and Proteus-KDO-NAGLIPASYN-PWY, and the SCFA-related Lactococcus-PWY-5677 and Lactococcus-PWY-5100. This pattern is consistent with the proposed functional direction but does not demonstrate metabolite production, pathway activation, or host effects. Citrobacter-P461-PWY and Citrobacter-P163-PWY have a nominal relationship and have not passed the correction. Since the bacterial genus and pathway values come from the same 16S input, the network is still an internal consistency analysis.

GDSC2 screening provides experimental prioritization layers. By ranking STAD cell line sensitivity, AZD2014, GNE-317, AZD5363, Uprosertib and GSK2110183B are at the top of the current list. These compounds can be used for subsequent functional validation, but tumor cell viability screens cannot model the full effects of macrophage activation, cytokine biology, microbial metabolites, radiotherapy, or immune checkpoint blockade; Translational interpretation requires co-culture, organoid, animal or clinical validation.

Public data comparisons are valuable ecological references. The significant pairwise alpha difference and beta results indicate that tissue status and treatment path cannot be confused. Exiguobacterium overlaps with the default filter set but Citrobacter does not.

The single cell layer enhances the explanatory power of cells mainly at the descriptive level: Annotation was based on marker inference, paired normal-tumor testing was limited to 4 patients, and 42 module tests were all unadjusted to significance. CellChat reveals a broad landscape of ECM and immune communication. Quasi-temporal ordering of cells along a state continuum. Neither type of analysis can demonstrate treatment-specific cellular remodeling or temporal sequencing .

Exiguobacterium was prioritized for inclusion because its four sets of orientations and abundance patterns were consistent with the RCI-pCR branch, and its associated fermentation and cell wall/PAMP pathways were derived from PICRUSt2 and retained as a deterministic association after multiple correction.

The main limitations define the boundaries of the conclusions: The cohort is cross-sectional after treatment, the RCI subgroup is small, and there is a lack of pre-treatment controls; Key confounders such as antibiotics, PPIs, Helicobacter pylori, sampling site, and sampling time were not available. PICRUSt2 cannot replace metagenomic sequencing or measured metabolome; TCGA and single cells are not derived from the same patient, and GDSC2 does not represent immuno-microbial pharmacology. Therefore, this study should be positioned as a linkage analysis of treatment paths to produce a structured verification route.

5. Conclusion

RCI and CI are associated with different but not drastic post-treatment gastric cancer microbial status. Citrobacter is the most robust genus with therapeutic associations. Four-group testing, independent tissue benchmarks, and external single-cell analysis enhance ecological and host context but do not turn the study into a causal or same-patient multi-omics empirical study. pCR within RCI was associated with higher Shannon and directional candidates, but no RCI species emerged as robust response biomarkers after multiple calibration; CI shows independent Lactococcus reaction association. PubMed query limited 4 low-explored LDA bacterial genera, among which Exiguobacterium is the main candidate in the RCI-pCR direction and is connected to the predicted fermentation/cell wall/PAMP pathway. When combined with independent host context layers, the results define three layers of testable microenvironmental hypothese.

The final framework is a testable closed loop: Therapeutic pathway-related microbiota characteristics → Predict acetate/SCFA and cell wall/PAMP functional cues → Independent tissue and host cell context → Experimental priority compounds. This closed loop is used to generate hypotheses and does not prove that

radiotherapy causes the observed microbial status, changes in acetate or other metabolites, that mTORC2-RhoA-NLRP3 is activated in the patient, that the CellChat ligation is therapeutically specific, or that either sequenced compound improves treatment response.

Declarations

Informed consent: Informed consent was obtained from all patients.

Consent for Publication: Not Applicable.

Clinical trial number: Not Applicable.

Ethics approval: All procedures in this study were in accordance with ethical standards of the institutional and national research committee and with the Helsinki Declaration of 1964 and later versions. This study was approved by the Ethics Committee of the Affiliated Cancer Hospital of Nanjing Medical University(reference number:2023-037).The plan reference number is neoACR for G/GEJ

Data availability: Processed 16S rRNA abundance tables, four-group stratification results, ellipse coordinates and overlap metrics, LDA outputs, PubMed taxa-screen and pathway-link tables, public cancer/non-cancer tissue benchmark tables, PICRUSt2-predicted functional profiles, single-cell QC and annotation tables, CellChat communication links, epithelial pseudotime tables, model output tables, the genus-level taxon result table with group medians, detection rates, effect sizes, confidence intervals, q values, ALDEx2 status, and sensitivity stability, the Exiguobacterium three-layer evidence ledger, figure source data, and analysis scripts are provided as separate Additional files accompanying this manuscript. De-identified clinical variables are included where permitted by institutional and privacy restrictions. Raw sequencing files and additional clinical information are not deposited in a public repository because they contain potentially sensitive patient-related information; they may be made available by the corresponding author upon reasonable request and subject to institutional approval(Data has been reposited in GEO https://dataview.ncbi.nlm.nih.gov/object/PRJNA1552657?reviewer=7u7cfhkkrc9dq5po1mcminlbee).

External transcriptomic data were obtained from the publicly available TCGA-STAD PanCancer Atlas resource through cBioPortal, and the external single-cell data were obtained from GEO accession GSE167297. The independent gastric tissue benchmark was derived from the public 16S dataset PRJNA532731 and its supplementary tables. Public pathway and metabolite annotations were derived from PICRUSt2/MetaCyc, KEGG, gutMGene, VMH/AGORA, CIDB, and related curated resources. PubMed literature counts were obtained through the NCBI E-utilities interface using the query and date recorded in the source-data tables. No same-cohort metabolomics data were generated in this study.

Author Contributions: Conceptualization: L.L.H., G.L., P.R., J.Y.G.; Writing - review and editing: G.L., R.P., J.Y.G., Z.W., and Y.S.; Project administration: M.R. and T.T.L. All authors have read and agreed to the published version of the manuscript.

Funding: This work was supported by the Research Project of Jiangsu Cancer Hospital (No. XCIS202401, RCQY202501, and ZBDL202502), the Yishan Research Project of Jiangsu Cancer Hospital (No. YSZD202404), the Qunfeng Project of Jiangsu Cancer Hospital (No. GFXK202503), and the Jiangsu Province 333 Project High-Level Talent Training Program (No. 2024-3-2249).

Conflict of interest: All authors declare no conflicts of interest.

References

1. Leite, L.F., et al., *Is pathological complete response a surrogate for overall survival in neoadjuvant clinical trials for gastroesophageal adenocarcinoma?* European journal of cancer (Oxford, England : 1990), 2026. **237**: p. 116602.
2. Tang, Z., et al., *The Neo-PLANET phase II trial of neoadjuvant camrelizumab plus concurrent chemoradiotherapy in locally advanced adenocarcinoma of stomach or gastroesophageal junction.* Nature communications, 2022. **13**(1): p. 6807.
3. Ma, X., et al., *Efficacy and safety of neoadjuvant chemoradiotherapy combined with immunotherapy for locally advanced esophagogastric junction or gastric cancer: a systematic review and meta analysis.* Frontiers in immunology, 2026. **17**: p. 1745356.
4. Li, X., et al., *Locally advanced gastroesophageal junction cancer with pathological complete response to neoadjuvant therapy: a case report and literature review.* Annals of translational medicine, 2021. **9**(6): p. 513.
5. Lin, J.-X., et al., *Perioperative camrelizumab and apatinib combined with chemotherapy for locally advanced gastric cancer in China: three-year survival outcomes of phase 2 randomized controlled trial.* EClinicalMedicine, 2025. **89**: p. 103568.
6. Badgwell, B., et al., *Phase 1 Trial of Total Neoadjuvant Therapy With Short-Course Chemoradiotherapy Followed by Chemotherapy for Patients With Potentially Resectable Gastric Cancer.* International journal of radiation oncology, biology, physics, 2025. **121**(2): p. 423–431.
7. Liang, H., *[Surgical strategies of radical gastrectomy for gastric cancer in the era of immunotherapy].* Zhonghua wei chang wai ke za zhi = Chinese journal of gastrointestinal surgery, 2025. **28**(9): p. 964–968.
8. Lordick, F., et al., *Adjuvant immunotherapy in patients with resected gastric and oesophagogastric junction cancer following preoperative chemotherapy with high risk for recurrence (ypN+ and/or R1): European Organisation of Research and Treatment of Cancer (EORTC) 1707 VESTIGE study.* Annals of oncology : official journal of the European Society for Medical Oncology, 2025. **36**(2): p. 197–207.
9. Chi, L., et al., *Comparative effectiveness of perioperative strategies for resectable gastric and gastroesophageal junction cancer: a Bayesian network meta-analysis.* American journal of cancer research, 2025. **15**(8): p. 3781–3794.
10. Huang, D., et al., *Perioperative immune checkpoint inhibitors combined with chemotherapy versus chemotherapy for locally advanced, resectable gastric or gastroesophageal junction adenocarcinoma: A systematic review and meta-analysis of randomized controlled trials.* International immunopharmacology, 2024. **138**: p. 112576.
11. Han, Y., et al., *Chemotherapy combined with immunotherapy in patients with gastric cancer: protocol for a systematic review.* BMJ open, 2024. **14**(12): p. e086986.
12. Xu, H., et al., *Evaluation of neoadjuvant immunotherapy plus chemotherapy in Chinese surgically resectable gastric cancer: a pilot study by meta-analysis.* Frontiers in immunology, 2023. **14**: p. 1193614.
13. Nakayama, I., M. Ohashi, and S. Nunobe, *Perioperative or neoadjuvant chemotherapy for locally advanced gastric or gastroesophageal junction cancer: from independent evidence in the West, the East, and Japan to global collaboration.* Chinese clinical oncology, 2024. **13**(1): p. 8.
14. Lordick Obermannová, R., et al., *Perioperative systemic therapy as a part of comprehensive multimodal treatment in esophageal and gastric cancer - new treatment guidelines.* Rozhledy v chirurgii : mesicnik Ceskoslovenske chirurgicke spolecnosti, 2024. **103**(11): p. 443–453.
15. Yıldız, İ., et al., *Current trends in perioperative treatment of resectable gastric cancer.* World journal of gastrointestinal surgery, 2023. **15**(3): p. 323–337.
16. Khan, U. and M.A. Shah, *Optimizing Therapies in the Perioperative Management of Gastric Cancer.* Current treatment options in oncology, 2019. **20**(7): p. 57.

17. Spencer, C.N., et al., *Dietary fiber and probiotics influence the gut microbiome and melanoma immunotherapy response.* Science (New York, N.Y.), 2021. **374**(6575): p. 1632–1640.
18. Baruch, E.N., et al., *Fecal microbiota transplant promotes response in immunotherapy-refractory melanoma patients.* Science (New York, N.Y.), 2021. **371**(6529): p. 602–609.
19. Cao, M., et al., *Single-cell transcriptomic analysis reveals gut microbiota-immunotherapy synergy through modulating tumor microenvironment.* Signal transduction and targeted therapy, 2025. **10**(1): p. 140.
20. Morder, K.M., et al., *Sucralose Consumption Ablates Cancer Immunotherapy Response through Microbiome Disruption.* Cancer discovery, 2025. **15**(11): p. 2278–2297.
21. Wong-Rolle, A., et al., *Unexpected guests in the tumor microenvironment: microbiome in cancer.* Protein & cell, 2021. **12**(5): p. 426–435.
22. Dubey, S.R., et al., *Molecular mechanisms and regulation of inflammasome activation and signaling: sensing of pathogens and damage molecular patterns.* Cellular & molecular immunology, 2025. **22**(11): p. 1313–1344.
23. Li, S., et al., *Short-chain fatty acids and cancer.* Trends in cancer, 2025. **11**(2): p. 154–168.
24. Mann, E.R., Y.K. Lam, and H.H. Uhlig, *Short-chain fatty acids: linking diet, the microbiome and immunity.* Nature reviews. Immunology, 2024. **24**(8): p. 577–595.
25. Yang, H.-J., *[Gastric Cancer and Gastric Microbiome].* The Korean journal of gastroenterology = Taehan Sohwagi Hakhoe chi, 2023. **81**(6): p. 235–242.
26. Coker, O.O., et al., *Mucosal microbiome dysbiosis in gastric carcinogenesis.* Gut, 2018. **67**(6): p. 1024–1032.
27. Kim, H.-N., et al., *Altered Gastric Microbiota and Inflammatory Cytokine Responses in Patients with Helicobacter pylori-Negative Gastric Cancer.* Nutrients, 2022. **14**(23).
28. Kim, M.-J., et al., *Combined DNA Methylation and Gastric Microbiome Marker Predicts Helicobacter pylori-Negative Gastric Cancer.* Gut and liver, 2024. **18**(4): p. 611–620.
29. Lv, X., et al., *Live bacteria found in gastric cancer tumor tissue.* Frontiers in microbiology, 2025. **16**: p. 1591735.
30. Rolling, T., et al., *Customization of a DADA2-based pipeline for fungal internal transcribed spacer 1 (ITS1) amplicon data sets.* JCI insight, 2022. **7**(1).
31. Callahan, B.J., et al., *DADA2: High-resolution sample inference from Illumina amplicon data.* Nature methods, 2016. **13**(7): p. 581–3.
32. Luo, H., et al., *EasyAmplicon 2: Expanding PacBio and Nanopore Long Amplicon Sequencing Analysis Pipeline for Microbiome.* Advanced science (Weinheim, Baden-Wurttemberg, Germany), 2026. **13**(1): p. e12447.
33. Singh, M.G. and R. Wahengbam, *Optimization of DADA2 in QIIME2 for improving fidelity in 16S rRNA V4 amplicon data analysis.* Biology methods & protocols, 2026. **11**(1): p. bpag002.
34. Douglas, G.M., et al., *PICRUSt2 for prediction of metagenome functions.* Nature Biotechnology, 2020. **38**(6): p. 685–688.
35. Blander, J.M. and G. Barbet, *Exploiting vita-PAMPs in vaccines.* Current opinion in pharmacology, 2018. **41**: p. 128–136.
36. Chen, H., et al., *mTORC2 controls Th9 polarization and allergic airway inflammation.* Allergy, 2017. **72**(10): p. 1510–1520.
37. Gulhati, P., et al., *mTORC1 and mTORC2 regulate EMT, motility, and metastasis of colorectal cancer via RhoA and Rac1 signaling pathways.* Cancer research, 2011. **71**(9): p. 3246–56.
38. Chiarello, M., et al., *Ranking the biases: The choice of OTUs vs. ASVs in 16S rRNA amplicon data analysis has stronger effects on diversity measures than rarefaction and OTU identity threshold.* PloS one, 2022. **17**(2): p. e0264443.
39. Gunathilake, M., et al., *Association between bacteria other than Helicobacter pylori and the risk of gastric cancer.* Helicobacter, 2021. **26**(5): p. e12836.
40. Zaramella, A., et al., *Predictive Value of a Gastric Microbiota Dysbiosis Test for Stratifying Cancer Risk in Atrophic Gastritis Patients.* Nutrients, 2024. **17**(1).
41. Sheh, A. and J.G. Fox, *The role of the gastrointestinal microbiome in Helicobacter pylori pathogenesis.* Gut microbes, 2013. **4**(6): p. 505–31.
42. Ziemski, M., et al., *MOSHPIT: accessible, reproducible metagenome data science on the QIIME 2 framework.* bioRxiv : the preprint server for biology, 2025.

43. Srivastava, A., Y. Akhter, and D. Verma, *A step-by-step procedure for analysing the 16S rRNA-based microbiome diversity using QIIME 2 and comprehensive PICRUSt2 illustration for functional prediction.* Archives of microbiology, 2024. **206**(12): p. 467.
44. Zou, X., et al., *Comparison of databases useful for the analysis of vaginal microbiota in Japanese women using next-generation sequencing data (QIIME 2 software).* Journal of applied microbiology, 2023. **134**(12).
45. Bai, J., et al., *Pilot Study of Vaginal Microbiome Using QIIME 2™ in Women With Gynecologic Cancer Before and After Radiation Therapy.* Oncology nursing forum, 2019. **46**(2): p. E48–E59.
46. Vétizou, M., et al., *Anticancer immunotherapy by CTLA-4 blockade relies on the gut microbiota.* Science, 2015. **350**(6264): p. 1079–1084.
47. Pardoll, D.M., *The blockade of immune checkpoints in cancer immunotherapy.* Nature Reviews Cancer, 2012. **12**(4): p. 252–264.
48. Ribas, A. and J.D. Wolchok, *Cancer immunotherapy using checkpoint blockade.* Science, 2018. **359**(6382): p. 1350–1355.
49. Sivan, A., et al., *Commensal Bifidobacterium promotes antitumor immunity and facilitates anti-PD-L1 efficacy.* Science, 2015. **350**(6264): p. 1084–1089.
50. Furusawa, Y., et al., *Commensal microbe-derived butyrate induces the differentiation of colonic regulatory T cells.* Nature, 2013. **504**(7480): p. 446–450.
51. Matson, V., et al., *The commensal microbiome is associated with anti-PD-1 efficacy in metastatic melanoma patients.* Science, 2018. **359**(6371): p. 104–108.
52. Stuart, T., et al., *Comprehensive Integration of Single-Cell Data.* Cell, 2019. **177**(7): p. 1888–1902.e21.
53. Callahan, B.J., et al., *DADA2: High-resolution sample inference from Illumina amplicon data.* Nature Methods, 2016. **13**(7): p. 581–583.
54. Tanoue, T., et al., *A defined commensal consortium elicits CD8 T cells and anti-cancer immunity.* Nature, 2019. **565**(7741): p. 600–605.
55. Spencer, C.N., et al., *Dietary fiber and probiotics influence the gut microbiome and melanoma immunotherapy response.* Science, 2021. **374**(6575): p. 1632–1640.
56. Davar, D., et al., *Fecal microbiota transplant overcomes resistance to anti-PD-1 therapy in melanoma patients.* Science, 2021. **371**(6529): p. 595–602.
57. Baruch, E.N., et al., *Fecal microbiota transplant promotes response in immunotherapy-refractory melanoma patients.* Science, 2021. **371**(6529): p. 602–609.
58. Subramanian, A., et al., *Gene set enrichment analysis: a knowledge-based approach for interpreting genome-wide expression profiles.* Proceedings of the National Academy of Sciences of the United States of America, 2005. **102**(43): p. 15545–15550.
59. Routy, B., et al., *Gut microbiome influences efficacy of PD-1-based immunotherapy against epithelial tumors.* Science, 2018. **359**(6371): p. 91–97.
60. Gopalakrishnan, V., et al., *Gut microbiome modulates response to anti-PD-1 immunotherapy in melanoma patients.* Science, 2018. **359**(6371): p. 97–103.
61. Trompette, A., et al., *Gut microbiota metabolism of dietary fiber influences allergic airway disease and hematopoiesis.* Nature Medicine, 2014. **20**(2): p. 159–166.
62. Hanahan, D. and R.A. Weinberg, *The hallmarks of cancer.* Cell, 2000. **100**(1): p. 57–70.
63. Hanahan, D., *Hallmarks of Cancer: New Dimensions.* Cancer Discovery, 2022. **12**(1): p. 31–46.
64. Hanahan, D. and R.A. Weinberg, *Hallmarks of cancer: the next generation.* Cell, 2011. **144**(5): p. 646–674.
65. Postow, M.A., M.K. Callahan, and J.D. Wolchok, *Immune checkpoint blockade in cancer therapy.* Journal of Clinical Oncology, 2015. **33**(17): p. 1974–1982.
66. Kroemer, G., et al., *Immunogenic cell death in cancer therapy.* Annual Review of Immunology, 2013. **31**: p. 51–72.
67. Kroemer, G., et al., *Immunogenic cell stress and death.* Nature Immunology, 2022. **23**(4): p. 487–500.
68. Hao, Y., et al., *Integrated analysis of multimodal single-cell data.* Cell, 2021. **184**(13): p. 3573–3587.e29.
69. Demaria, S., et al., *Ionizing radiation inhibition of distant untreated tumors (abscopal effect) is immune mediated.* International Journal of Radiation Oncology, Biology, Physics, 2004. **58**(3): p. 862–870.
70. Ritchie, M.E., et al., *limma powers differential expression analyses for RNA-sequencing and microarray studies.* Nucleic Acids Research, 2015. **43**(7): p. e47.
71. Arpaia, N., et al., *Metabolites produced by commensal bacteria promote peripheral regulatory T-cell generation.* Nature, 2013. **504**(7480): p. 451–455.
72. Sepich-Poore, G.D., et al., *The microbiome and human cancer.* Science, 2021. **371**(6536): p. eabc4552.

73. Mager, L.F., et al., *Microbiome-derived inosine modulates response to checkpoint inhibitor immunotherapy.* Science, 2020. **369**(6510): p. 1481–1489.
74. Helmink, B.A., et al., *The microbiome, cancer, and cancer therapy.* Nature Medicine, 2019. **25**(3): p. 377–388.
75. Roy, S. and G. Trinchieri, *Microbiota: a key orchestrator of cancer therapy.* Nature Reviews Cancer, 2017. **17**(5): p. 271–285.
76. Love, M.I., W. Huber, and S. Anders, *Moderated estimation of fold change and dispersion for RNA-seq data with DESeq2.* Genome Biology, 2014. **15**(12): p. 550.
77. Galluzzi, L., et al., *Molecular mechanisms of cell death: recommendations of the Nomenclature Committee on Cell Death 2018.* Cell Death & Differentiation, 2018. **25**(3): p. 486–541.
78. Hato, S.V., et al., *Molecular pathways: the immunogenic effects of platinum-based chemotherapeutics.* Clinical Cancer Research, 2014. **20**(11): p. 2831–2837.
79. Liberzon, A., et al., *The Molecular Signatures Database (MSigDB) hallmark gene set collection.* Cell Systems, 2015. **1**(6): p. 417–425.
80. Bolyen, E., et al., *Reproducible, interactive, scalable and extensible microbiome data science using QIIME 2.* Nature Biotechnology, 2019. **37**(8): p. 852–857.
81. Mann, E.R., Y.K. Lam, and H.H. Uhlig, *Short-chain fatty acids: linking diet, the microbiome and immunity.* Nature Reviews Immunology, 2024. **24**(8): p. 577–595.
82. Formenti, S.C. and S. Demaria, *Systemic effects of local radiotherapy.* The Lancet Oncology, 2009. **10**(7): p. 718–726.